Synthesis of stable Pb based perovskite nanocrystals and plasmonic hollow nanoparticles

Tinku Ram Meena

MS14125

A dissertation submitted for the partial fulfilment of BS-MS dual degree in Science

Indian Institute of Science Education and Research Mohali
April 2019

Certificate of Examination

This is to certify that the dissertation titled **Synthesis of stable Pb based perovskite nanocrystals and plasmonic hollow nanoparticles s**ubmitted by **Mr. Tinku Ram Meena (Reg. No. MS14125)** for the partial fulfillment of BS-MS dual degree programme of the Institute, has been examined by the thesis committee duly appointed by the Institute. The committee finds the work done by the candidate satisfactory and recommends that the report be accepted.

Dr. Sanchita Sengupta Dr. Monika Sharma Dr. Debrina Jana
(Supervisor)

Declaration

The work presented in this dissertation has been carried out by me under the guidance of Dr. Debrina Jana at the Indian Institute of Science Education and Research Mohali. This work has not been submitted in part or in full for a degree, a diploma, or a fellowship to any other university or institute. Whenever contributions of others are involved, every effort is made to indicate this clearly, with due acknowledgement of collaborative research and discussions. This thesis is a bonafide record of original work done by me and all sources listed within have been detailed in the bibliography.

Tinku Ram Meena
(Candidate)
Date:

In my capacity as the supervisor of the candidate's project work, I certify that the above statements by the candidate are true to the best of my knowledge.

Dr. Debrina Jana
(Supervisor)

Acknowledgement

I would like to express my sincere gratitude to my thesis supervisor Dr. Debrina Jana for her constant support and encouragement throughout the period of my MS thesis. I am feeling blessed for submitting my master thesis under her guidance.

I gratefully acknowledge INSPIRE faculty research grant (DST/INSPIRE/04/2015/002741) from DST, Govt. of India for funding this work and DST for INSPIRE-SHE fellowship.

I would like to express thanks to my project committee members Dr. Sanchita Sengupta and Dr. Monika Sharma for their valuable discussion and suggestions that improved contents of this dissertation.

I would like to thank IISER Mohali for the research facilities, for GIXRD characterization, CSIR-CGCRI, IIT Mandi and INST for TEM characterization. I also thank Mr. Vivek Singh for taking FE-SEM images of all my samples.

I am really grateful to my lab members Isabella, Parth, Samita, Daimiota and Shikha for creating a healthy and cheerful environment in the lab.

I feel blessed to have Suresh Kumar, Yogendra Sharma, Neetish Kumar Sharma, Vishal Tiwari, Apoorv Alawada, Shubham Bhojane and Ravi Kumar in my life. Their love and support keeps me happy always.

Last but the most significant, it gives me immense pleasure to express my gratitude to my beloved **parents and family members** who have always believed in me and supported with unconditional love throughout my life. I want to thank god for giving me this interesting life and amazing parents.

List of Figures

List of Tables

Notations and Abbreviations

PNCs	Perovskite Nanocrystals
DMF	N,N-Dimethylformamide
ASB	Aluminium-Tri-Sec-Butoxide
CTAB	Cetyl trimethyl ammonium bromide
EG	Ethylene Glycol
PVP	Polyvinyl Pyrollidone
NPs	Nanoparticles
AA	Ascorbic acid
DEG	Diethylene Glycol
$PbBr_2$	Lead Bromide
CsBr	Cesium Bromide
GA	Gallic acid
Pd	Palladium
HCl	Hydrogen Chloride
Br	Bromine
NaHS	Sodium hydrosulfide hydrate
NCs	Nanocrystals

CONTENTS

ABSTRACT

Perovskite nanocrystals (PNCs) have emerged as potential candidate for photovoltaic and light harvesting devices owing to their excellent optoelectronic properties. However, working on nanoscale of these perovskite nanocrystals has been a challenge due to several factor including stability, high temperature requirement, moisture dependency, requirement of inert medium and agglomeration tendency of the nanocrystals. Our main emphasis is to produce stable $CsPbBr_3$ nanocrystals inside wormhole mesoporous alumina thin film. These $CsPbBr_3$ nanocrystals shows tunable blue and green emission. Choice of suitable solvents and precursor incorporation sequence enables generation of $CsPbBr_3$ nanocrystals at room temperature inside mesoporous alumina film whereas tunable emissive property can be attributed to the size increment of the nanocrystals promoted by differing precursor concentration.

Noble metal nanoparticles have attracted interest of researchers due to their optical properties. Plasmon resonance can be controlled by their size and shape. Our main focus is to synthesize different shaped Pd nanoparticles and study the role of shape in catalysis. Ag nanoparticle has been used in solution based single molecule SERS, but their usage is limited due to toxicity and oxidation issue. Au nanoparticle is biocompatible and SERS active, but they show less SERS enhancement factors. Therefore silver core-gold shell NPs can be alternative for single molecule SERS. Our focus is to synthesize hollow Ag core Au shell nanoparticle and study their potentiality for ultrasensitive SERS detection of biomolecules.

Chapter 1: Introduction

1.1 Project 1

1.1.1 Perovskite Nanocrystals (PNCs)

The general formula for perovskites is AMX_3 where A is the cation which can be organic or inorganic (Cs^+, $CH_3NH_3^+$, $CH_3(NH_2)^{2+}$; M is the divalent metal cation part (Pb^{2+}, Sn^{2+}, Ge^{2+}); X is the anion (Cl^-, Br^-, I^-).[1] Figure 1 shows the arrangement of the atoms in a cubic crystal.

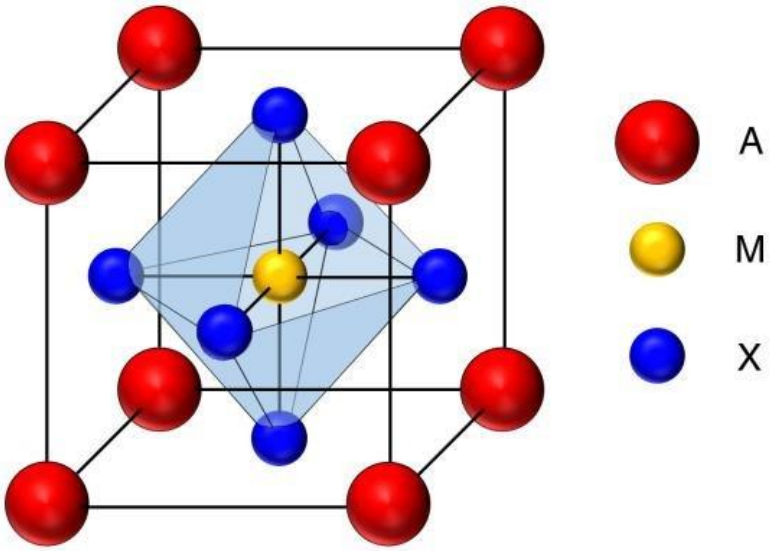

Figure 1. Perovskite (AMX_3) cubic crystal structure of cations and anions (taken from ref. 2).

Perovskite nanocrystals (PNCs) have emerged as potential candidate for photovoltaic and light harvesting devices owing to their excellent optoelectronic properties. Superior charge transport property, tunable band gap by compositional change,

narrow emission band with high quantum efficiencies as well as improved stability than organic counterparts have been achieved in case of all-inorganic PNCs.[3]

1.1.2 Tuning of Photoluminescence (PL)

1.1.2.1 Halide exchange

$CsPbX_3$ NCs exhibits bright luminescence with high quantum yield upto 90% and narrow emission wavelengths that were tuned over entire the visible region depending on the NCs size and halide ion composition.[3]

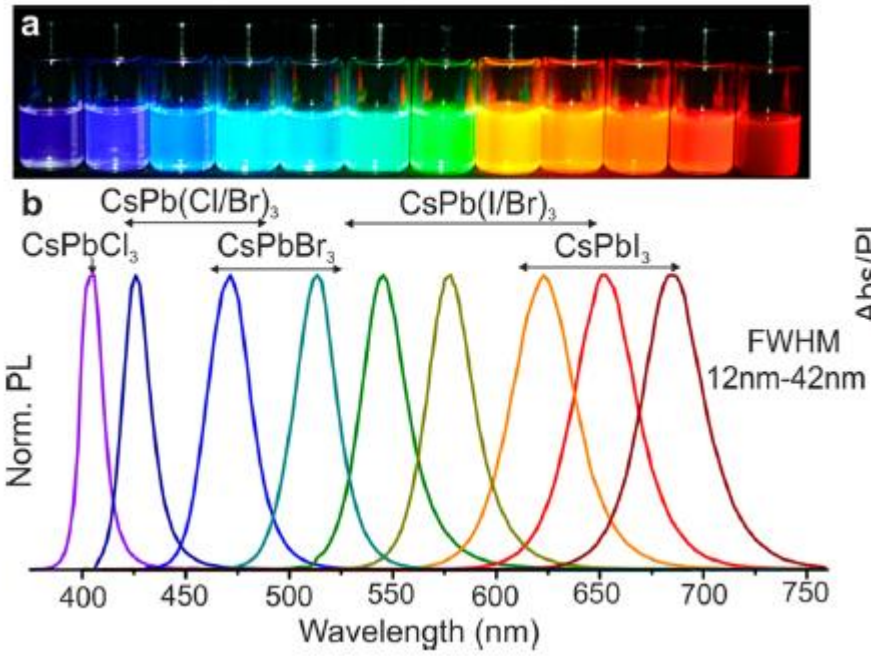

Figure 2. Colloidal perovskite $CsPbX_3$ NCs (X = Cl, Br, I) exhibit size- and composition-tunable bandgap energies covering the entire visible spectral region with narrow and bright emission λ = 365 nm (taken from ref. 3).

1.2.1.2 Doping

Doping with transition metal ion (Mn^{2+}) is another way of tuning the PL. Doping with transition metal ions has been extensively explored as a way to introduce new optical, electronic, and magnetic properties, making them much more functional than their undoped counterparts.[4]

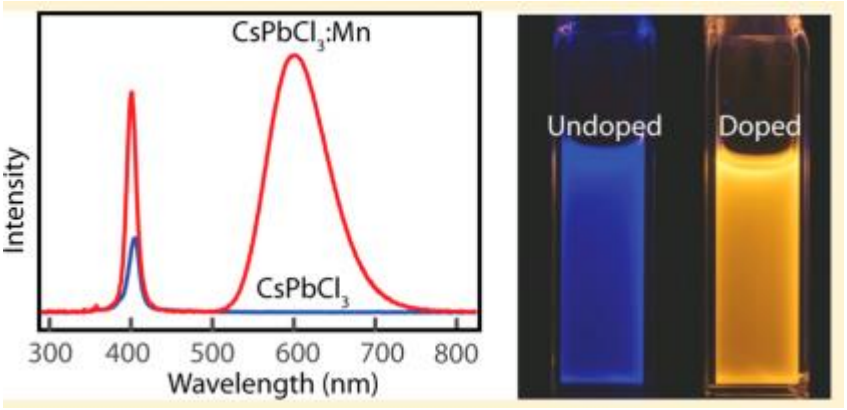

Figure 3. Photoluminescence of Mn-doped and undoped $CsPbCl_3$ NCs (taken from ref. 4).

1.1.2 My approach

Colloidal solution form of synthesized perovskite nanocrystals is well known method to synthesize PNCs which includes injection of the two precursor's solution in inert atmosphere at high temperature. Solution based synthesis has poor stability and inhomogeneity in the size and shape limits its applicability[5]. Mesoporous powder assisted way of synthesis different shaped nanocrystals to tune the emission spectra over the entire visible region has been reported.[14] Alternative way of synthesizing PNCs is vapor assisted method for making film, but using this method we cannot control the size of PNCs. Our goal is to develop uniform mesoporous alumina film template and synthesis of PNCs inside the mesopores. In same mesoporous alumina template we want to tune the size of PNCs which may can tune the emission wavelength. Template assisted method increases the stability of PNCs due to confinement of the nanocrystals inside the mesopores. Advantage of template method is that we do not require high temperature, capping agent, inert atmosphere and it also prevent agglomeration of the nanocrystals.

Project 2

1.2.1 Plasmonic nanoparticle and Surface Plasmon Resonance (SPR)

Origin of surface plasmon resonance in noble metal nanoparticles (NPs) is the free electrons in the metal (d electrons in silver and gold) are free to travel through the material. The mean free path in gold and silver is around 50 nm, therefore in particles smaller than this, scattering is not expected from the bulk. Thus, all interactions are expected to be with the surface. Light in resonance with the surface plasmon oscillation results in the oscillation of free-electrons in the metal. The resonance condition is determined from absorption and scattering spectroscopy and is found to depend on the shape, size, and dielectric constants of both the metal and the surrounding material. The dielectric constant changes on changing the solvent, but the shape is most important in determining the shift of the plasmon resonance.[6] Changing the shape from a sphere to rod or hexagon or star like shape of NP will change its SPR drastically and thus remains the basis of ultrasensitive detection of molecules.[6]

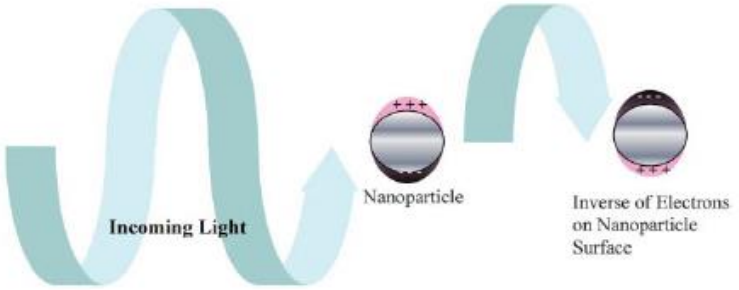

Figure 4. Origin of surface plasmon resonance due to coherent interaction of the electrons in the conduction band with light (taken from ref. 6).

1.2.2 Tuning of SPR by coupling NPs or making NP with hollow interior

When a pair of plasmonic nanoparticles comes together, their plasmon fields couple and a enhanced field is generated, which is more intense than the individual plasmon

field intensity of the single particle as we can see in figure 6.[7] Coupling of plasmon field in case of solid and hollow NP is different from each other. Effect of wall thickness and separtion distance of Au nanoframes on plasmonic field can be seen in figure 6.

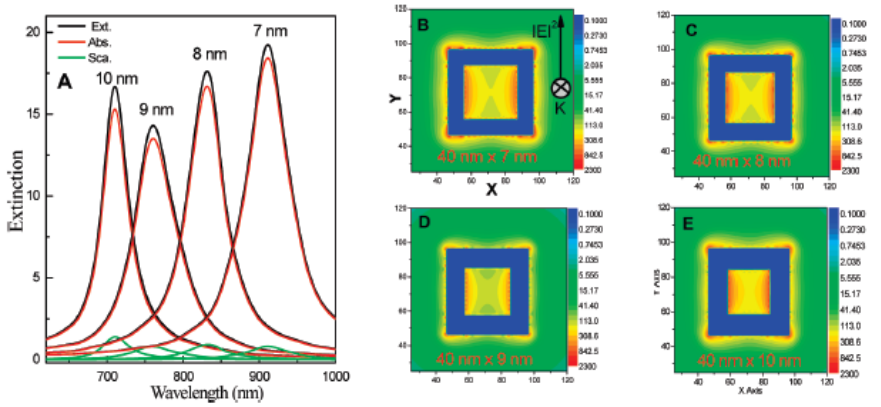

Figure 5. Tuning of SPR by altering the wall thickness of a hollow interior NP (taken from ref. 7).

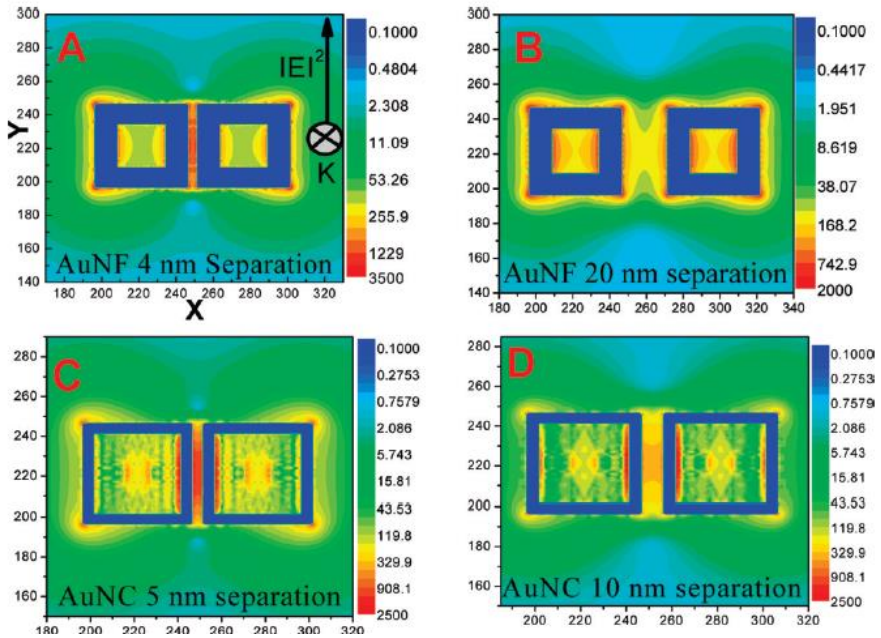

Figure 6. (A,B) 40 nm Au nanoframe with wall thickness of 10 nm, placed at separation of 4 and 20 nm, (C,D) 50 nm Au nanocage with wall thickness of 5 nm, placed at separation of 5 and 10 nm (taken from ref. 7).

1.2.3 My Approach

There are many solution phase experiments in SERS, which are performed using either Ag or Au nanoparticles. Though Ag nanoparticle shows better enhancement in Raman intensities but they are not biocompatible, while Au NPs are biocompatible but shows moderate enhancement in Raman intensities[18,20]. Hollow NPs show better Raman enhancement than solid one.[19] By taking care of above mentioned condition, we want to synthesize hollow Ag core Au shell (Ag@Au) NPs using solid Ag NPs as template. My goal is to explore the potentiality of hollow Ag@Au NPs towards achieving single molecule sensitivity using SERS.

Chapter 2

Experimental Section

2.1 Chemicals

Palladium acetate [$Pd(OAc)_2$], Polyvinylpyrrolidone PVP-55, (MW 55,000), Tannic acid, Cetyl trimethyl ammonium bromide (CTAB), Diethylene glycol, Ethylene glycol, Aluminum-tri-sec-butoxide (ASB), Pluronic F127, Sodium hydrosulfide hydrate (NaSH), Silver Trifluoroacetate (CF_3COOAg) and $PbBr_2$ were taken from Sigma Aldrich. 1-propanol ($CH_3CH_2CH_2OH$), and methanol were obtained from s. d. fine-chem limited and Ranbuxy fine chemicals. CsBr (99.9%) and N,N-Dimethylformamide (DMF, 98%) were purchased from Alfa-Aesar and SRL Pvt. Ltd. respectively. Hydrochloric acid (HCl, 37% emparta) and Acetone (99%) from Merck and SRL used respectively. Gallic acid was purchased from Lobachemie. Ascorbic acid of SRL were used. Coumarin 540A was obtained from Exciton. Milli-Q water obtained from the Millipore water purification system was used for all purposes. All glass wares were thoroughly cleaned with aqua regia, washed with Milli-Q water and dried in hot air oven before use. All chemicals were used as received without any further purification.

2.2 Methods

2.2.1 Synthesis of perovskite

For preparation of boehmite sol, Yoldas method was followed which involves hot hydrolysis (>80 °C) of ASB and subsequent peptization of boehmite precipitates using HCl.[8] The molar ratios of water/ASB and HCl/ASB were 100 and 0.10, respectively.

After peptization, the sol was stirred vigorously in refluxing condition for 5 h and then kept for another 48 h under refluxing condition without stirring. The product from the above reflux "Sol", was concentrated to about 7.5 wt % of $AlO_{1.5}$ content by distilling off the butan-2-ol and some portion of water. In order to bring the $AlO_{1.5}$ content to 5.3 wt% required amount of methanol was added. Further, mesoporous alumina films were prepared from boehmite sol using F127 as structure directing agent. A calculated amount of F127 (such that it reaches 0.001 mol per mol of $AlO_{1.5}$) was dissolved in 1-propanol after that boehmite sol was added to it. $AlO_{1.5}$ content at this stage was maintained at 4 wt% and micellar arrangement forms inside the sol. This sol was used for preparation of the films on glass slides using dip-coating method by single dipping technique. The prepared (as discussed above) films were dried initially at 60 °C in a hot-air oven. Surfactant from the films were removed by calcination at 500 °C (ramp of 2 °C min^{-1} with a holding time of 60 min) in case of glass substrates whereas ethanol extraction method was used for flexible polypropylene and polyethylene terephthalate sheets. In this way, mesoporous alumina film was formed on the glass slide/polypropylene sheet. For generation of PNCs inside the mesoporous film matrix, two-step dipping procedure was undertaken. First, the mesoporous alumina film was dipped into 0.025-0.5 M $PbBr_2$ solution in DMF with a holding time of 2 min and withdrawal speed was maintained at 140 mm/s. This film was kept in air for about 45 s before washing it in DMF solvent, followed by oven drying for 15 min at 60 °C. 0.025-0.5 M solution of CsBr was prepared in water: ethanol mixture (1.5/6.5 as v/v), and stirred for 30 min. After bringing down the oven dried film to room temperature (by keeping in open air for some time), it was dipped in CsBr solution with a holding time of 30 seconds.[1] Withdrawal speed was maintained same and finally the slide was washed with ethanol and kept inside desiccator. Vacuum pump attached to the desiccator was kept switched on for 10 mins initially and then it was removed. The

slide was kept inside desiccator overnight in this condition and all the characterizations were done after this process.

2.2.2 Synthesis of differently shaped Pd NPs

2.2.2.1 With Ascorbic acid

In this synthesis, CTAB is used as a surfactant and capping agent, whereas ascorbic acid is used as mild reducing and shape directing agent. 3 mL water and 10 mL AA (63 mg) transferred in 100 mL RB flask. After that 5.6 mg of $Pd(OAc)_2$ dissolved in 1.5 mL of acetone separately and added to the RB flask.[21] Then this reaction mixture was put on an electric heating mantle with refluxing apparatus. After 3-4 min 91 mg of CTAB dissolved in 10 mL water was added in above reaction and this reaction mixture kept for 45 min at 85±1 °C.

2.2.2.2 With Gallic acid

In this synthesis, CTAB is used as a surfactant and capping agent, whereas gallic acid is used as mild reducing and shape directing agent. 3 mL water and 10 mL AA (63 mg) transferred in 100 mL RB. After that 5.6 mg of $Pd(OAc)_2$ dissolved in 1.5 mL of acetone separately and added to the RB flask. Then this reaction mixture was put on an electric heating mantle with refluxing apparatus. After 3-4 min 91 mg of CTAB dissolved in 10 mL water was added in above reaction and this reaction mixture kept for 45 min at 85±1 °C.

2.2.3 Synthesis of silver cube

2.2.3.1 Synthesis of silver cube (size 20-25 nm)

In this synthesis, 5 mL of DEG was added into 30 ml vial and heated under magnetic stirring in an oil bath set to 150 °C for 30 min.[9] All other reactants were separately dissolved in DEG and sequentially introduced into the flask using pipet. Sequentially, 0.006 mL (60 µL) of NaSH solution (3 mM) was added first. After 4 min, 0.5 mL of HCl (3 mM) was added, followed by 1.25 mL of PVP (20 mg/mL). After 2 min, 0.4 mL of CF_3COOAg solution (282 mM) was added and further this solution was kept for 3 hour at

150 °C. During the entire process, the flask was capped with glass stoppers except for the addition of reactants. The synthesis was quenched by placing the flask in an ice-water bath and the products were diluted with acetone and collected by centrifugation. After this it was washed twice with distilled water to remove the remaining precursor, DEG, and excess PVP. At last it was re-dispersed in distilled water.

2.2.3.2 Synthesis of silver cube (size 70-80 nm)

In this synthesis, 5 mL of EG was added into a flask and heated under magnetic stirring in an oil bath set to 150 °C for 30 min. [10] All other reagents separately dissolved in EG and sequentially introduced into the flask using pipet. Sequentially, 0.006 mL (60 μL) of NASH solution (3 mM) was added first. After 4 min, 0.5mL of HCl (3 mM) was added, followed by 1.25 mL of PVP (20 mg/mL). After 2 min, 0.4mL of CF_3COOAg solution (282 mM) was added, the resultant solution was kept for 90 min at 150 °C. During the entire process, the flask was capped with glass stoppers except for the addition of reactants. The synthesis was quenched by placing the flask in an ice-water bath and the products were diluted with acetone and collected by centrifugation. After this it was washed twice with distilled water to remove the remaining precursor, DEG, and excess PVP. At last it was re-dispersed in distilled water.

2.2.4 Synthesis of hollow Ag @ Au Cube

0.5 mL of prepared Ag cube converted to 2 mL by added 1.5 mL water. 0.5 mL Ag cube was taken from above diluted solution in 20 mL vial. These 0.5 mL Ag NPs dispersed in 3 mL of distilled water containing 1mg/mL PVP-55(MW-55000) and heated to 90 °C. After 4-5 min specific amount of $HAuCl_4$ (10^{-3} M) added and kept for 30 min.[9] The synthesis was quenched by placing the vial in an ice- water bath, then products were collected by centrifugation.

2.4 Materials characterization

2.4.1 Scanning Electron Microscopy

The morphology of all the Pd, Ag, Ag @ Au NPs was observed by using Field Emission Scanning Electron Microscopy (FE-SEM) JEOL-7600F. All the samples Were drop casted on cleaned Silicon wafer and then kept in oven to evaporate solvent after that images were recorded. The FE-SEM was operated with an acceleration voltage of 5-15 KV and a chamber pressure of 10^{-5} torr.

2.4.2 UV-Visible Spectroscopy

UV-visible spectra of the films deposited on silica/quartz glass substrates and Ag/Au nanoparticle were measured using Cary 5000 UV-Vis NIR (Agilent Technologies) spectrophotometer at the scan rate of 1 nm/s. Quartz cuvette of path length 1 cm at room temperature was used for recording the optical spectra. Baseline correction with corresponding solvent was done every time to eliminate the effect of solvent in the spectrum.

2.4.3 Photoluminescence Spectroscopy

Photoluminescence (PL) spectra were recorded at an excitation wavelength λ_{ex} = 400 nm using Horiba Fluromax-4. For all the samples slit widths were kept at 1 nm x 1.5 nm with an scan integration time of 0.5 s.

2.4.4 TCSPC Measurement

Horiba Fluorohub-B used for PL lifetime measurements at an excitation wavelength of 375 nm using a pico second diode laser at a repetition rate of 1 Mhz. The instrument response function (IRF) was recorded using 1% ludox (colloidal silica) solution.

2.4.5 Grazing incidence X-ray diffraction (GIXRD)

Grazing incidence X ray diffraction (GIXRD) pattern of the thin films were recorded by Rigaku Smartlab GIXRD machine using Cu Kα (λ≈1.54059 Å) radiation operating at 9 kW (tube current 200 mA and tube voltage 45 kV) equipped with a rotating anode. X-ray intensity was enhanced using cross-beam optics. Grazing incidence angle was maintained at 0.3 °.

2.4.6 Transmission electron microscopy (TEM)

Transmission electron microscopic (TEM) measurements were carried out with Tecnai G^2 30ST (FEI) and Tecnai G^2 20 STWIN (FEI) equipped with energy dispersive X-ray scattering (EDS) facility. For TEM sample preparation, scratched off coatings were dispersed in acetone and drop casted onto the carbon-coated grid.

2.4.7 Profilometer

The thickness of the coatings was measured by a Surfcorder SE-2300 profilometer (Kosaka Laboratory Ltd., Japan).

2.4.8 Raman Spectroscopy

Raman spectroscopy is equipped with three lasers (514 nm, 633 nm, 785 nm). We mixed both Ag NPs and 10^{-4} M Nile blue solution, then we recorded spectra using 5X lens and 785 nm laser source.

Chapter 3

Results and Discussion

3.1 Perovskite

Wormhole mesoporous films on glass substrates were formed by dip-coating technique from a boehmite sol where the surfactant F127 was added to form the micellar structure. As coated samples were subjected to oven drying at 60 °C, followed by gradual heat treatment to 500 °C for one hour, which leads to the generation of wormhole mesopores in ~1 μm thick alumina film.

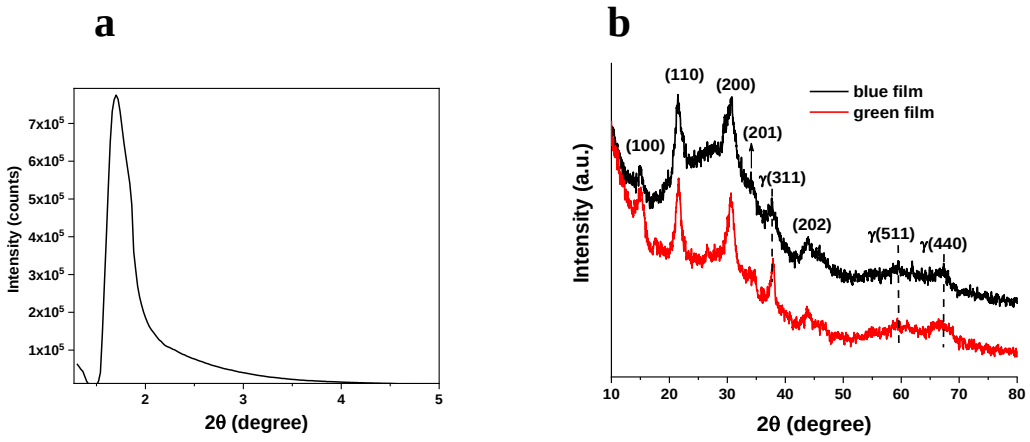

Figure 7. (a) Low angle XRD of γ-Al_2O_3 film shows broad peak indicating the existence of disordered mesopores. (b) GIXRD of the films showing the formation of cubic $CsPbBr_3$ NCs inside nanocrystalline γ-Al_2O_3 thin film. Peaks corresponding to γ-Al_2O_3 has been indicated by putting a 'γ' sign before the planes.

Alumina coated galss slide first dipped in $PbBr_2$ solution (dissolved in DMF) for 2 min. After drying in oven, second dipping was done in CsBr solution (dissolved in water:ethanol mixture as 1.5/6.5 v/v). Using lower concentration of $PbBr_2$ solution (0.025 M) leads to the generation of blue luminescence whereas higher one (0.1 M) yields green emission (will be designated as blue and green film respectively hereafter). Concentration of CsBr was kept constant at 0.1 M for both cases. Low angle (Figure 7a) and high angle GIXRD (Figure 7b) confirm the presence of disordered mesopores[11] and formation of γ-Al_2O_3 phase respectively (JCPDS card 10-0425).[12] Broad nature of high angle peaks of γ-Al_2O_3 suggests nanocrystalline nature of the film matrix.[13] GIXRD of both the films confirm the formation of cubic $CsPbBr_3$ phase (JCPDS card 54-0752 Figure 7b).[22]

N_2-sorption analyses were previously carried out to evaluate the surface area and the porosity of the γ-Al_2O_3 as well as $CsPbBr_3$ NCs-Al_2O_3 composite film.[1] Surface area of the γ-Al_2O_3 and $CsPbBr_3$ NCs-Al_2O_3 composite film (green film was taken as representative) was found to be 139 and 117.4 m^2g^{-1} respectively. Decrement of surface area indicates filling of pores by $CsPbBr_3$ NCs which is further confirmed form the pore volume data. Total pore volume of the γ-Al_2O_3 and $CsPbBr_3$ NCs-Al_2O_3

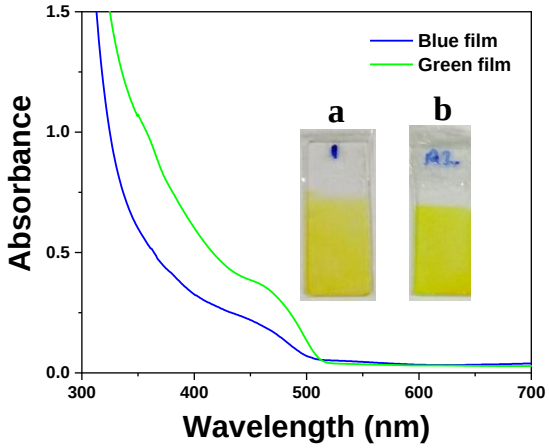

Figure 8. UV-visible spectra of the $CsPbBr_3$ NCs-Al_2O_3 composite films. Inset shows the digital image of a) blue and b) green film at day light.

Composite film was evaluated to be 0.2 and 0.141 cm^3 respectively which indicates 30% decrement of pore volume happens due to pore filling by the perovskite NCs. Average pore size (~4 nm) calculated from the adsorption bench of the isotherm fells well in the mesoporous region.

UV-visible spectrum of the $CsPbBr_3$ NCs-Al_2O_3 composite film and digital image of the film at day light has been shown in Figure 8.

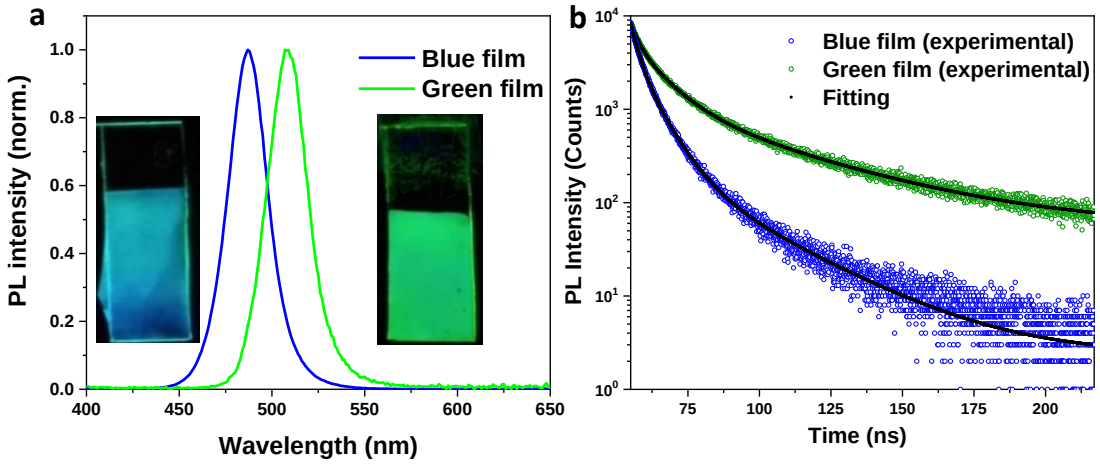

Figure 9. (a) PL spectra of blue and green films, inset shows the digital photo of the films (b) Time-resolved PL decay (λ_{ex} = 375 nm) of blue and green films.

PL spectra (Figure 9a) demonstrates the occurrence of maxima at 485 and 507 nm respectively for blue and green film and absence of any other additional peaks. Digital photos of both the films can be seen also. PL spectral maxima of both the films have been blue shifted compared to the bulk perovskite at 525 nm[15] which gives evidence of the quantum confinement for the NCs in thin film form. Full-widths-at-half-maximum (FWHMs) of emission peak (Emission linewidth of the film sample) is quite narrow, only 24 nm for blue and green film which indicates good crystal quality and also indicates that the contribution to PL is coming most likely from a narrow size range of NCs.[15] The photoluminescence decay curves of blue and green film are presented in Figure 9b. Decay dynamics is multi exponential and in agreement with previous results.[14] Average lifetimes range from 9-12 ns and 17-24 ns for multiple blue and green films respectively (see

Figure 10). These films show good quantum yield (~40% for both blue and green film) as compared to the bulk perovskite and powder.[14,15] Results corresponding to the photo physical study of the two samples have been incorporated in Table 1.

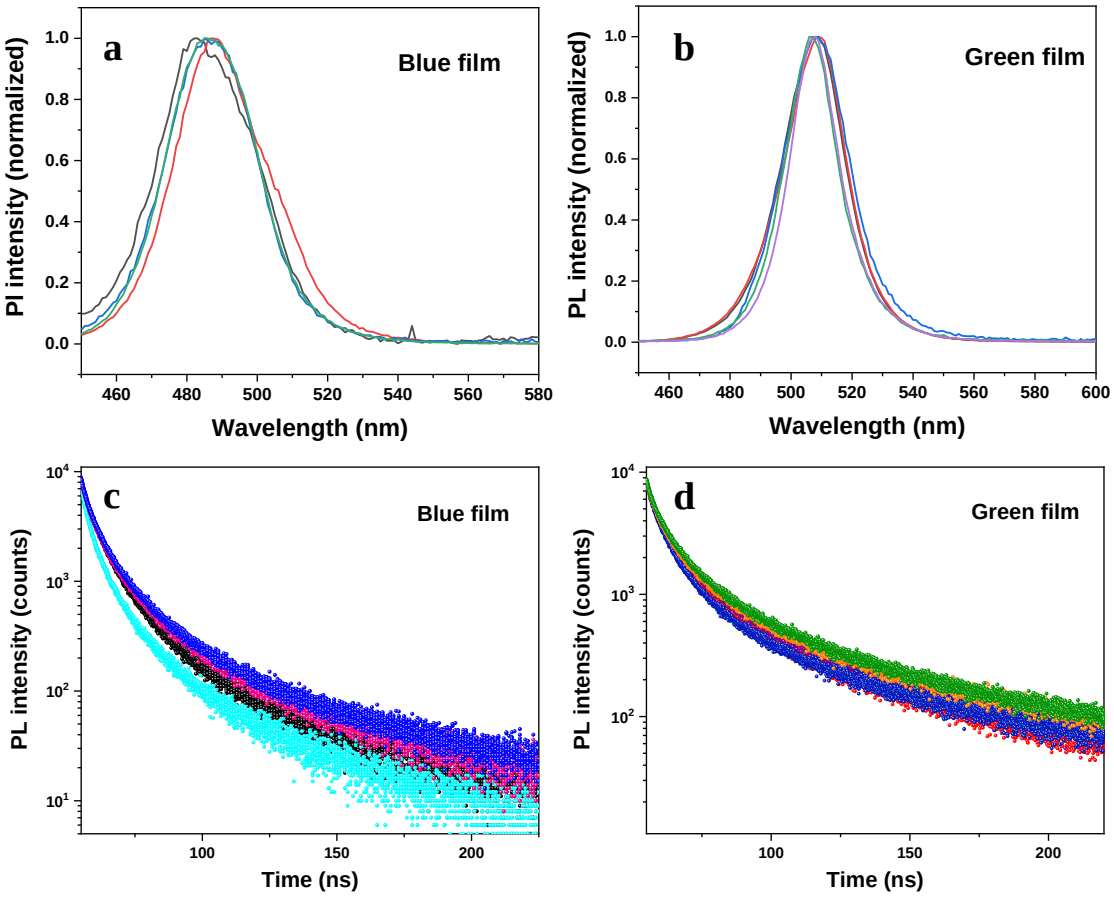

Figure 10. (a,b) Photoluminescence spectra and (c,d) decay curves of few blue and green films respectively on glass substrates. PL maxima of blue films range from 482-487 nm, whereas for green film 505-509 nm. Lifetimes range from 9-12 ns and 17-24 ns for blue and green films respectively.

To get insight into the PL emission tunability in the NCs, TEM study was undertaken to understand the NC morphology change, if any. Figure 11 shows the bright field TEM images of blue film. From Figure 11a, it is evident that mostly NCs in the size range of ~3-4.5 nm has been formed in this step. Particle size distribution was obtained from around 200 particles taken from different portions of the film with an average particle size of 3.86 nm (inset of Figure 11a). Narrow particle size distribution is in accord with the existence of a single sharp peak in PL spectra without any additional peak. Magnified image shows the crystalline nature of the γ-Al_2O_3 matrix as well as the existence of small $CsPbBr_3$ NCs (circled by yellow dots). HRTEM image of one such NC shows characteristic lattice fringes corresponding to (200) plane of $CsPbBr_3$. From the bright field TEM image (Figure 12) of the green film it is evident that NCs are bigger in size compared to the last one. Size increment explains the shifting of luminescence from blue to green as also evidenced by previous authors using colloidal synthetic route.

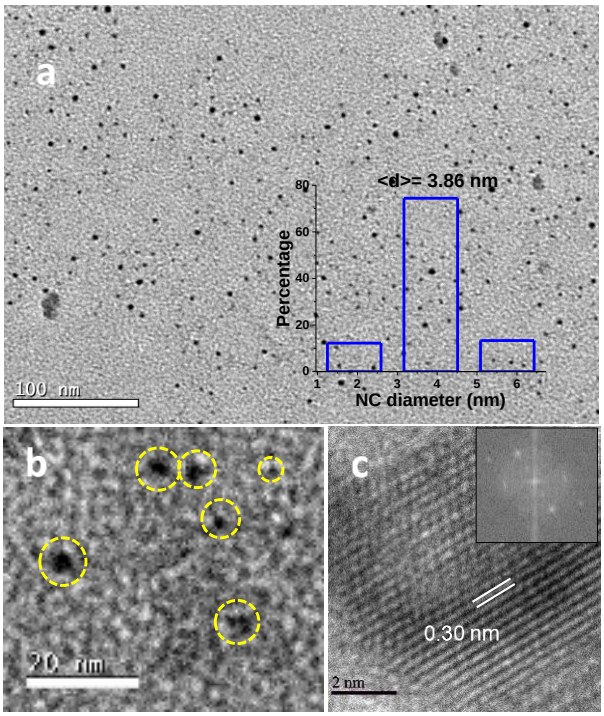

Figure 11. Bright field TEM images (a) showing the existence of $CsPbBr_3$ NCs inside blue film (particle size distribution has been shown in inset, average particle size is 3.86 nm), (b) higher resolution image showing crystalline γ-Al_2O_3 as matrix and small

NCs (circled by yellow dots) can be seen, (c) HRTEM of one NC shows the characteristic lattice fringes of (200) plane of cubic $CsPbBr_3$ NC (FFT shown in inset).

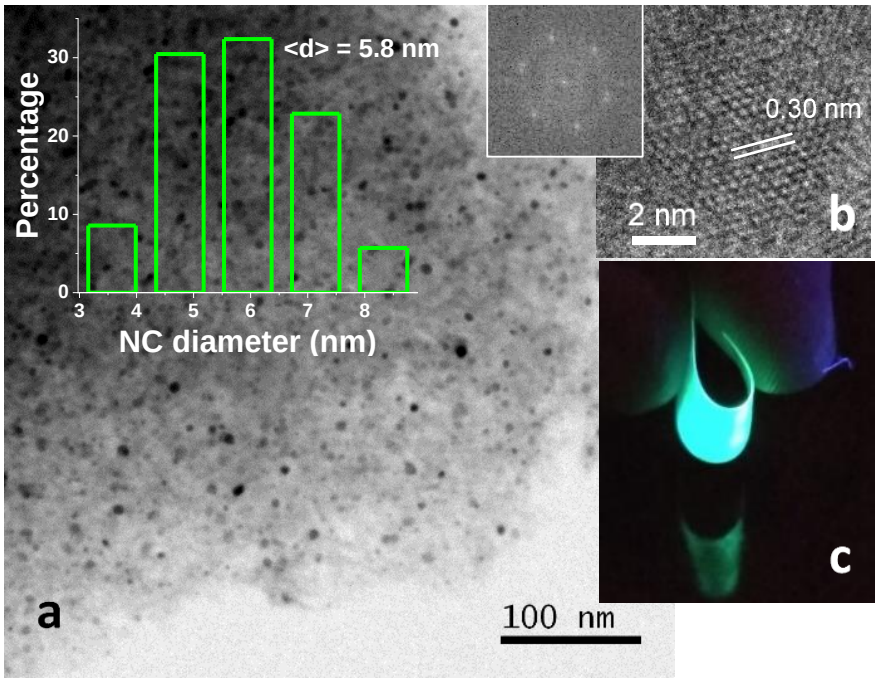

Figure 12. (a) Bright field TEM image showing the existence of $CsPbBr_3$ NCs in the green film, particle size distribution in the inset reveals maximum NCs are in the range of 4.5-7.5 nm with a mean size of 5.8 nm. (b) HRTEM of one NC shows the characteristic lattice fringes of (200) plane of cubic $CsPbBr_3$ NC (FFT shown in inset), (c) $CsPbBr_3$ NCs-Al_2O_3 composite film on flexible polypropylene substrate.

Further increment in concentration of $PbBr_2$ precursor solution retains the green colour luminescence. TEM study was also undertaken to visualize the size/shape of NCs at higher precursor concentration. As evident from Figure 13, the size of the NCs has been considerably increased. Mean size has been calculated as 13 nm, which indicates that concentration of precursor solution has profound effect on determining the size. Also, it can be understood that, higher concentration leads to the migration of bigger NCs towards the surface of films as a result of the compressive stress due to confinement inside the

pores. PL spectra from the films using higher concentration of precursor solutions show existence of two peaks indicating a mixed range of sizes of NCs (Figure 14).

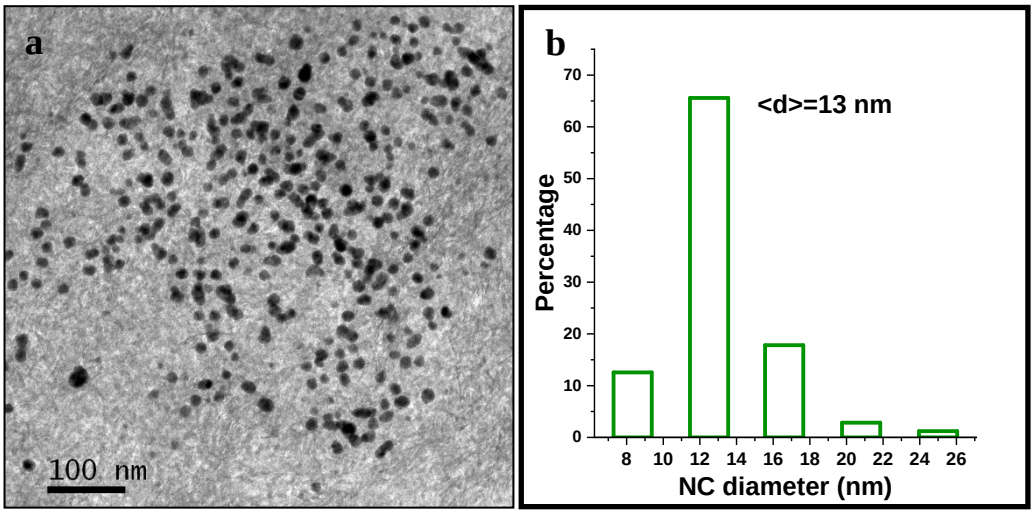

Figure 13. a) TEM image showing the formation of larger $CsPbBr_3$ NCs (mean particle size is 13 nm, as evident from (b) particle size distribution) inside γ-Al_2O_3 film while concentrations of precursors $PbBr_2$ and CsBr solutions were kept at 0.5 M and 0.1 M respectively.

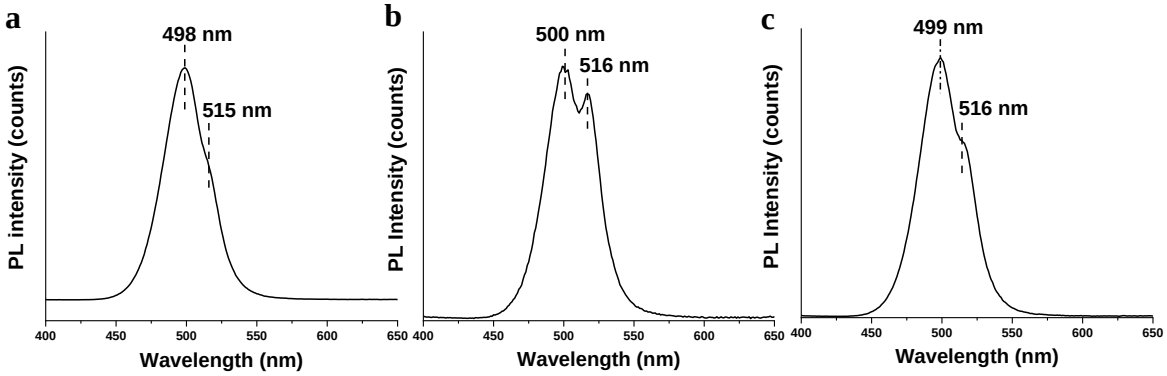

Figure 14. Photoluminescence spectra of few films (a-c) where higher concentrations of precursor solutions were used ($PbBr_2$ > 0.1 M, CsBr ≥ 0.1 M) for dipping. TEM image of one such combination has been shown in Figure 13.

This matrix offers advantages such as a) presence of extended interconnecting channels opens up innumerable pathways for precursor solution diffusion, b) wormhole mesopores allow similar extent of access of precursor solutions unlike the ordered mesopores[15] c) dewetting of the solution may take longer time than the ordered analogues, thus beneficial for interaction of the precursor solutions inside the pores. Smaller NCs are forming inside the pores depending on pore size and precursor concentration, leading to quantum confinement. Also, increment of precursor solution concentration facilitates more interaction of the as formed NCs with the remaining precursor solution, thereby leading to more coalescence and eventually larger NCs.

A major drawback for using perovskite NCs is their instability under ambient atmosphere. To check the stability of these composite films, multiple films were kept inside a petri dish in ambient atmosphere and PL and TCSPC characterizations were done from time to time. Figure 15 shows the data corresponding to the PL and TCSPC for such a film around a time scale of 8 months. For both blue and green films, PL emission spectra and life times do not show significant changes which indicates the superiority of this film towards better stability.

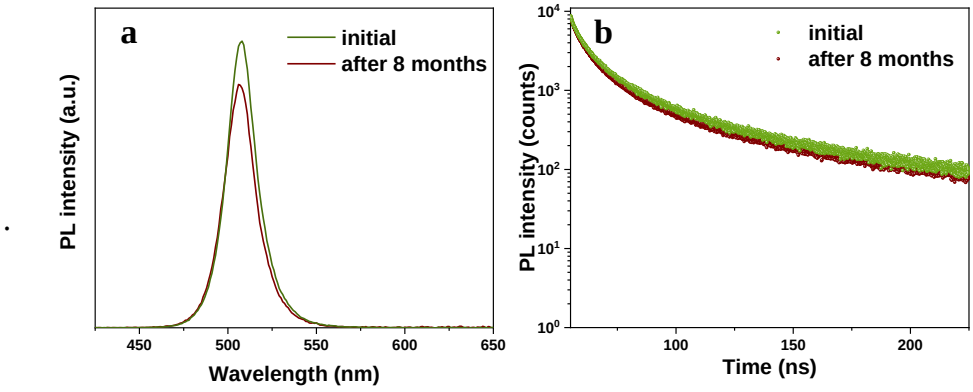

Figure 15. (a) PL spectra and (b) decay curves of $CsPbBr_3$ NCs-Al_2O_3 composite films: as prepared and after 8 months.

PL decay graphs were fitted using the tri-exponential function of the following form

$$A(t) = A_1 e^{-t/T_1} + A_2 e^{-t/T_2} + A_3 e^{-t/T_3}$$

Average lifetime $<T_L>$ is calculated as

$$< T_L > = \frac{A_1T_1^2 + A_2T_2^2 + A_3T_3^2}{A_1T_1 + A_2T_2 + A_3T_3}$$

Lifetime is calculated as

$$PL\ QY sample = \left(\frac{\Phi_{sample}}{\Phi_{reference}}\right)x\left(\frac{A_{reference}}{A_{sample}}\right)x\left(\frac{n_{sample}}{n_{reference}}\right)^2 x\ QY_{reference}$$

Radiative and non-radiative lifetime is calculated as

$$\text{PL QY} = \frac{<T_L>}{T_r} = \frac{T_{nr}}{T_r + T_{nr}}$$

Where, Φ_{sample} = Integrated Area under the PL emission curve of sample

$\Phi_{reference}$ = Integrated Area under the PL emission curve of reference

A_{sample} = Absorbance at excitation wavelength of sample

$A_{reference}$ = Absorbance at excitation wavelength of reference

n_{sample} = Refractive index of sample

$n_{reference}$ = Refractive index of reference

T_{nr} = Radiative lifetime (ns)

T_r = Non radiative lifetime (ns)

TABLE 1 Fitting parameter of PL decay graph and related calculation

Film type	T_1 (ns)	T_2 (ns)	T_3 (ns)	A_1 (%)	A_2 (%)	A_3 (%)	X^2	$<T_L>$ (ns)	PL QY (%)	T_r (ns)	T_{nr} (ns)
Blue film	4.49	15.43	1.033	50	22	28	1.13	10.59	41.32	25.63	18.05
Green film	6.35	25.34	1.34	48	23	29	1.20	18.08	42.00	43.06	31.18

For relative PL quantum yield (PL QY), same alumina film was soaked in 10^{-4} coumarin 540A dye solution (standard QY of 53%) in ethanol and was used as reference.[16]

3.2 Palladium nanoparticles

Palladium nanoparticles were synthesized by using palladium acetate as precursor, CTAB as capping agent and ascorbic and gallic acid as reducing agent as well as structure directing agent.

3.2.1 Ascorbic acid (AA) as reducing agent

Palladium acetate reacts with ascorbic acid and CTAB in water and gives monodispersed Pd nanoparticle as evident from FE-SEM image in figure 16. Ascorbic acid reduces Pd^{2+} to Pd^{0}. Exact shape of particle cannot be defined from FE-SEM image due to small size, so TEM characterization needs to be done.

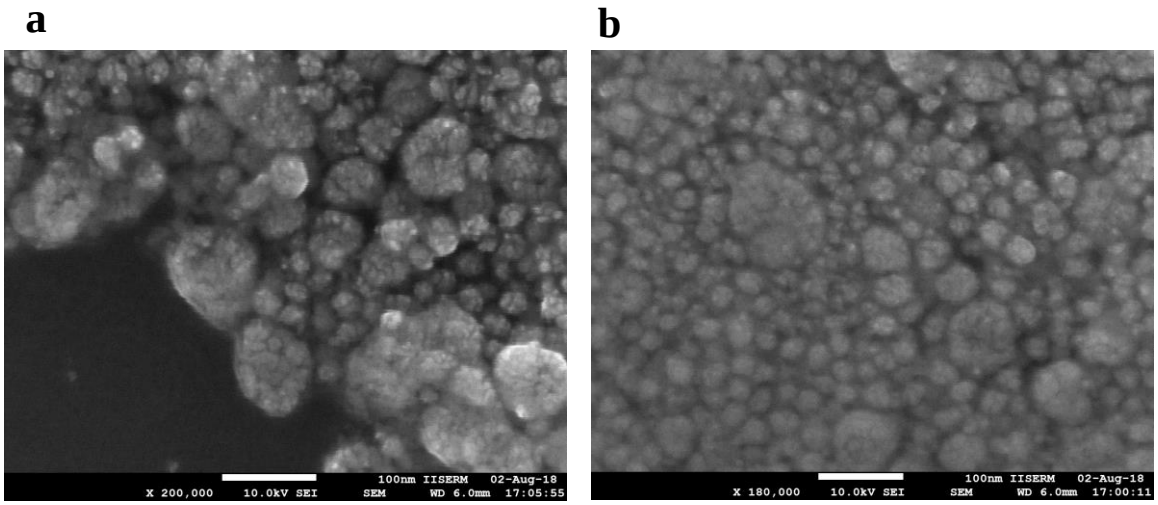

Figure 16. (a,b) FE-SEM image of the Pd NPs with ascorbic acid

CTAB is used as capping agent which prevents the agglomeration of Pd NPs and also control the shape of Pd NPs. CTAB has Br^{-1} as counter anion which play role in shape conversion because halide ion can do oxidative etching. Cl^{-1} shows better oxidative etching than Br^{-1} and etching tends to selectively start from defect side.[17]

3.2.1 Gallic Acid (GA) as reducing agent

Palladium acetate undergoes reaction with gallic acid and CTAB in water and gives monodispersed Pd NPs as evident from FE-SEM image in figure 17. Gallic acid reduces Pd^{2+} to Pd^{0}. Exact shape of particle cannot be defined from FE-SEM image due to small size, so TEM characterization needs to be done.

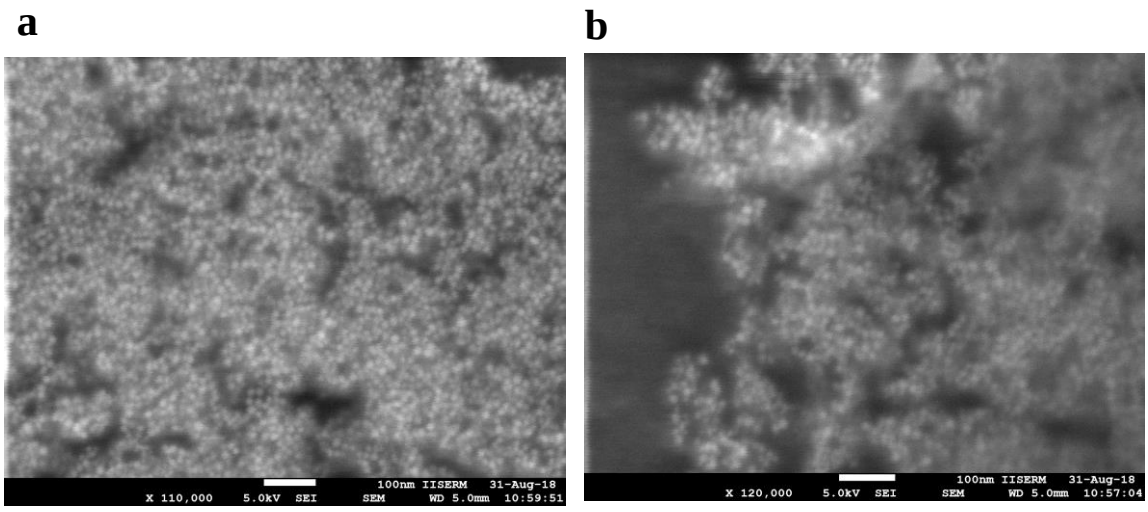

Figure 17. (a,b) FE-SEM image of the Pd NPs with gallic acid

CTAB is used as capping agent and gallic acid is used as reducing agent as well as structure directing agent. Capping agent and reducing agent both of them play role in shape conversion of Pd NPs. Size of these Pd NPs around 12 nm.

3.3 Silver and silver core gold shell NPs.

3.3.1 Silver cube

Silver cubes were synthesized using diethylene glycol as solvent and reducing agent, PVP is used as stabilizing agent. Silver trifluoroacetate is used as precursor. NaSH and HCl both played important role in synthesis of monodispersed cubic Silver NPs.[9]

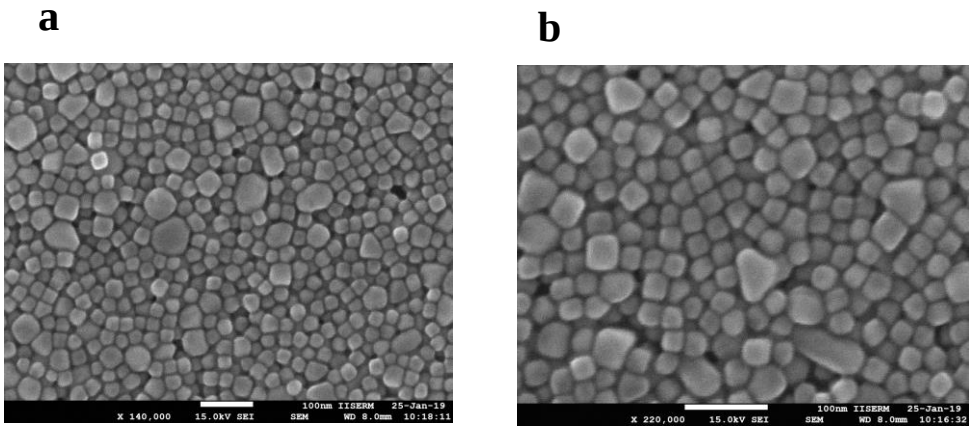

Figure 18. (a,b) FE-SEM image of silver cubic NPs (size 20-25 nm)

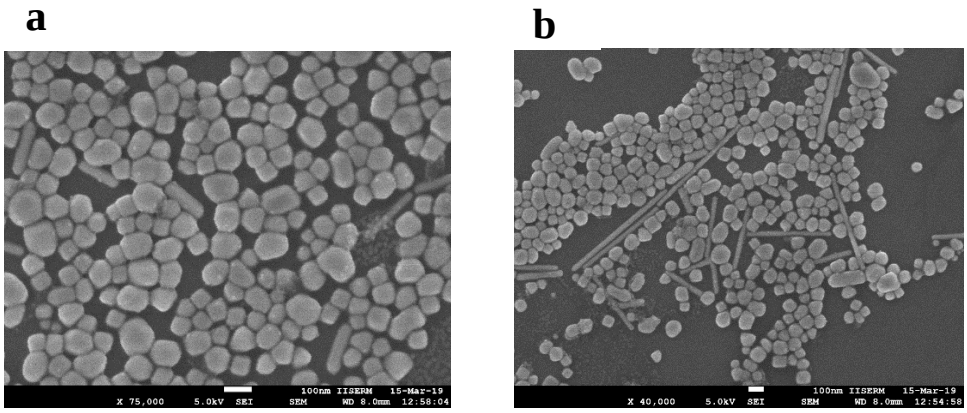

Figure 19. (a,b) FE-SEM image of silver cubic NPs (size 70-80 nm)

Size of small Ag cubic NPs is 20-25 nm as we see in figure 18, while size of bigger Ag cubes is 70-80 nm as we can see in figure 19.

When we changed diethylene glycol (DEG) to ethylene glycol (EG) which acts as both solvent and reducing agent, NPs of bigger size are observed.[9-10] DEG possess higher viscosity and lower reducing power relative to EG. Maximum absorbance peak is observed at 407 and 459 nm for small and large Ag cube respectively, increase in wavelength also confirms increment in size of Ag NPs as we can see in figure 20. Large Ag cubes are not that much monodispersed as small Ag cubes, more modification needs to be done to get monodispersed NPs.

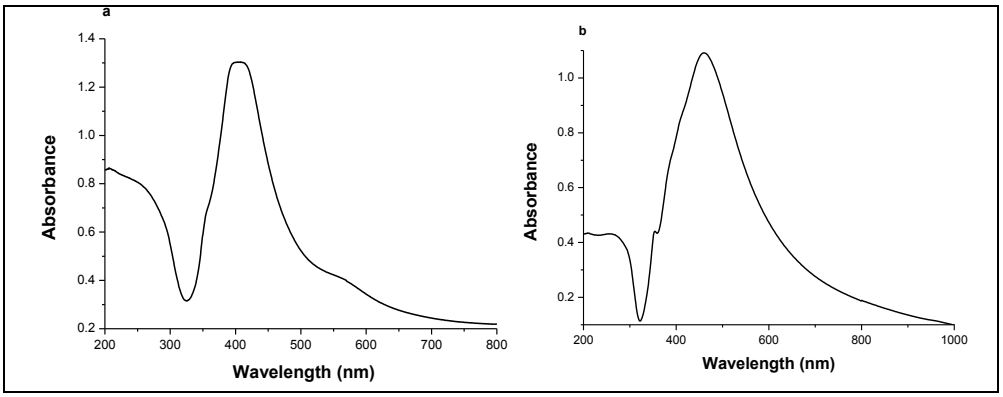

Figure 20. UV-Vis spectra of (a) small Ag cube (b) large Ag cubic NPs

3.3.2 Silver core gold shell (Ag@Au) NPs.

For synthesis of hollow Ag@Au NPs small Ag NPs is used as template and 3 mM $HAuCl_4$ solution was used. Here Ag and Au are in 0 and +3 oxidation state respectively. Reduction potential of silver (+1 to 0) and gold (+3 to 0) are 0.79 and 1.5 V respectively. Under the galvanic reaction silver get oxidized from 0 to +1 oxidation state while gold is reduced to 0 oxidation state from +3 oxidation state. As a result of this galvanic replacement reaction we got hollow Ag@Au NPs as we can see in figure 21. Optical property can be tuned by tuning volume of $HAuCl_4$ as we can see in figure 22.

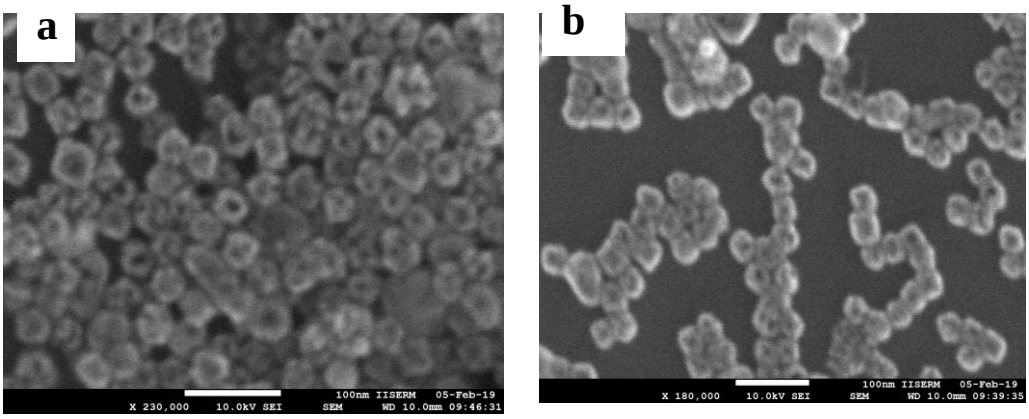

Figure 21. (a,b) FE-SEM image of hollow Ag @ Au NPs

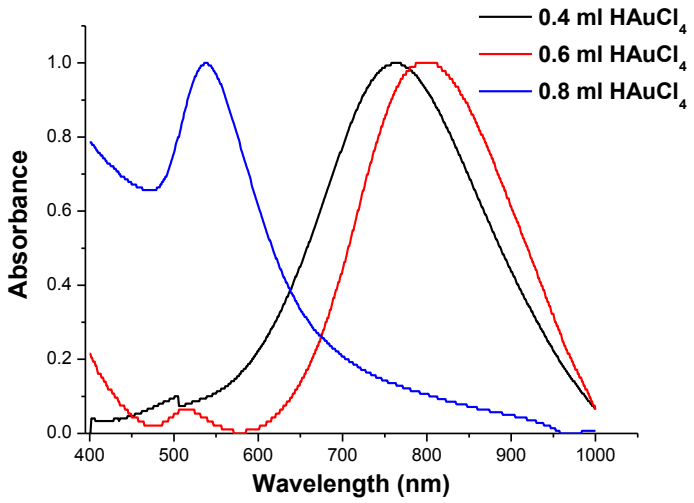

Figure 22. UV-Vis spectra of hollow Ag @ Au NPs prepared using different amount of $HAuCl_4$.

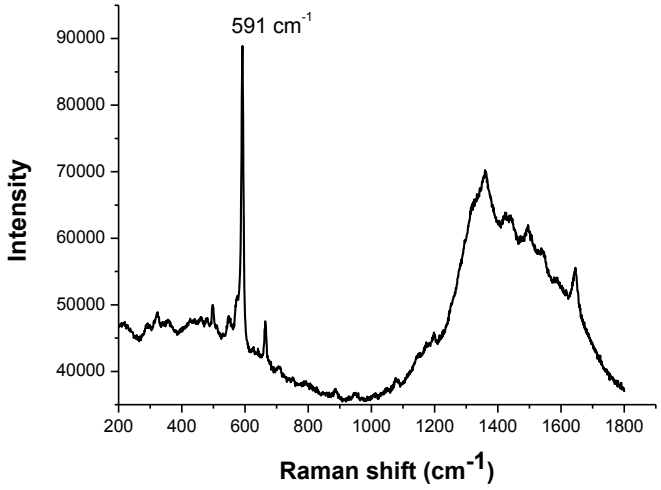

Figure 23. Raman spectrum of Nile blue dye (10^{-4} M).in presence of Ag cubic NPs.

Raman spectra of Nile blue dye (10^{-4} M) in presence of Ag cubic NPs is taken and the SERS spectra can be seen in figure 23. Characteristic Raman peak of the dye at 591 cm^{-1} can be seen to be enhanced in this condition.

Conclusion

We have successfully synthesized $CsPbBr_3$ NCs with tunable emission inside mesoporous γ-alumina thin film at room temperature. Wormhole mesoporous structure has been found to be effective towards the reproducible generation of blue and green emitting $CsPbBr_3$ NCs. Adjusting the concentration of precursor solutions regulates the size of NCs, thereby selectively generates PL emission inside the composite films, whereas employment of suitable solvents during the preparation procedure enables room temperature synthesis of NCs. Stability of the films towards light and moisture as supported by experimental evidences along with high PL QY will be advantageous for application in light emitting and light harvesting devices.

We have successfully synthesized silver cubic and hollow silver core gold shell NPs with tunable optical properties. Synthesis of different shaped palladium NPs were also done successfully.

Future work

Study of ultrasensitive SERS detection of biomolecule using silver core gold shell NPs will be undertaken. Catalysis study of different shaped palladium NPs is currently underway.

References

1. Takhellambam, D.; Meena, T. R.; Jana, D. *Chem. Commun.,* **2019**, *55*, 4785.
2. https://www.researchgate.net/profile/David_Giovanni/publication/325218134/figure/fig3/AS:627584266141699@1526639157551/Perovskite-generic-crystal-structure-The-cubic-crystal-structure-of-3D-perovskite.png.
3. Protesescu, L.; Bodnarchuk, S. M. I.; Krieg, F.; Hendon, R. C. H.; Yang, R. X.; Walsh, A.; Kovalenko, M. V. *Nano Lett.,* **2015**, *15*, 3692.
4. Parobek, D.; Roman, B. J.; Dong, Y. H. J.; Lee, E.; Sheldon, M.; Son D. H. *Nano Lett.*, **2016**, *16*, 7376.
5. Ravi, V. K.; Swarnkar, A.; Chakraborty, R.; Nag, A. *Nanotechnology* **2016**, *27*, 325708.
6. Eustis, S.; El-Sayed, M. A.; *Chem. Soc. Rev.,* **2006**, *35*, 209.
7. Mahmoud, M. A.; Snyder, B.; El-Sayed, M. A.; *J. Phys. Chem. C* **2010**, *114*, 7436.
8. Yoldas, B. E. *Am. Ceram. Bull.,* **1975**, *54*, 289.
9. Wang,Y.; Zheng, Y.; Huang, C. Z.; Xia, Y. *J. Am. Chem. Soc*. **2013**, *135*, 1941.
10. Zhang, Q.; Li,W.; Wen, L.P.; Chen, J.; Xia, Y. *Chem. Eur. J.* **2010**, *16*, 10234.
11. Deng, W.; Toepke, M. W.; Shanks, B. H. *Adv. Funct. Mater*., **2003**, *13*, 61; b) Cabrera, S.; Haskouri, J. E.; Beltran J. A.; eltran, B. D.; Mendioroz, S.; Marcos, M. D.; Amoros, P. *Adv. Mater.*, **1999**, *11*, 379.
12. Jana, D.; De, G. *Cryst. Growth Des.* **2019**, *19*, 1494.
13. Gregg,S. J.; Sing, K. S. W. in *Adsorption, surface area, and porosity,* New York: *Academic Press*, **1982**.
14. a) Dirin, D. N.; Protesescu, L.; Trummer, D.; Kochetygov, I. V.; Yakunin,S.; Krumeich, F.; Stadie ,N. P.; Kovalenko, M. V. *Nano Lett.* **2016**, *16*, 5866. b) Malgras, V.; Tominaka, S.; Ryan, J. W.; Henzie, J.; Takei, T. Ohara, K.; Yamauchi, Y. *J. Am. Chem. Soc.* **2016**, *138*, 13874. c) Anaya, M.; Rubino, A.; Rojas, T. C.; Galisteo-López, J. F.; Calvo, M. E.; Míguez, H. *Adv. Optical Mater.* **2017**, 5, 1601087, d) Chang, S.; Bai, Z.; Zhong, H. *Adv. Optical Mater.* **2018**, *6*, 1800380.
15. Malgras, V.; Henzie, J.; Takei, T.; Yamauchi, Y. *Angew. Chem. Int. Ed.* **2018**, *57*, 8881.

16. Grabolle, M.; Spieles, M.; Lesnyak, V.; Gaponik, N.; Eychmüller, A.; Resch-Genger, U. *Anal. Chem.* **2009**, *81*, 6285.
17. Zheng, Y.; Zeng, J.; Ruditskiy, A.; Liu, M.; Xia,Y. *Chem. Mater.* **2014**, *26*, 22.
18. Kumar, G. V. P.; Shruthi, S.; Vibha, B.; Reddy, B. A. A.; Kundu, T. K.; Narayana, C. *J. Phys. Chem. C* **2007**, *111*, 4388.
19. Mahmoud, M. A.; O'Neil, D.; El-Sayed, M. A. *Chem. Mater.* **2014**, *26*, 44.
20. Patra, P. P.; Kumar, G. V .P. *J. Phys. Chem. Lett.* **2013**, *4*, 1167.
21. Lee, Y. W.; Kim, M.; Han, S. W. *Chem. Commun*., **2010**, *46*, 1535.
22. Chen, M.; Zou, Y.; Wu, L.; Pan, Q.; Yang, D.; Hu, H.; Tan, Y.; Zhong, Q.; Xu, Y.; Liu, H.; Sun, B.; Zhang, Q. *Adv. Func. Mater*. **2017,** *27*, 1701121.